

| 1. AGENCY USE ONLY (Leave blank) | 2. REPORT DATE | 3. REPORT TYPE AND DATES COVERED |
|---|---|---|
| | May 10, 1993 | Reprint |

**4. TITLE AND SUBTITLE**
Characteristics of Suprathermal Electron Bursts Observed by the DMSP-F6/F7 Satellites in the Diffuse Aurora Region

**5. FUNDING NUMBERS**
PE 61102F
PR 2311
TA G5
WU 02

**6. AUTHOR(S)**
H. Nakajima*, H. Fukunishi*, T. Ono**, F.J. Rich

**7. PERFORMING ORGANIZATION NAME(S) AND ADDRESS(ES)**
Phillips Lab/GPSG
29 Randolph Road
Hanscom AFB, MA 01731-3010



**8. PERFORMING ORGANIZATION REPORT NUMBER**
PL-TR-93-2107

**9. SPONSORING/MONITORING AGENCY NAME(S) AND ADDRESS(ES)**

**10. SPONSORING/MONITORING AGENCY REPORT NUMBER**

**11. SUPPLEMENTARY NOTES** *Upper Atmosphere and Space Research Laboratory, Tohoku Univ. Sendai, 980, Japan **National Institute of Polar Research, Tokyo 173, Japan
Reprinted from J. Geomag. Geoelectr., 45, 1-22, 1993

**12a. DISTRIBUTION/AVAILABILITY STATEMENT**
Approved for public release; Distribution unlimited

**12b. DISTRIBUTION CODE**

**13. ABSTRACT** (Maximum 200 words)

The particle data of the DMSP-F6 and -F7 satellites show the presence of suprathermal electron bursts in the diffuse aurora region. These bursts are characterized by intense (~$10^8$–$10^9$ (cm$^2$sr sec)$^{-1}$), low energy (~100–500 eV), and localized (~20–30 km at satellite altitude $h$ = 830 km) electron precipitation. Simultaneous magnetic field data from the DMSP-F7 satellite show that these bursts are often, but not always, accompanied with intense (few $\mu$Am$^{-2}$), small-scale (only few tens of km at satellite altitude) upward field-aligned currents. The bursts are observed from 19 h to 11 h MLT through midnight during the maximum to recovery phase of substorm. These bursts are less likely to be observed during geomagnetic storms than during times of isolated substorms. These results suggest that suprathermal electron bursts are generated by localized heating of ionospheric electrons which flow out from the ionosphere toward the magnetosphere during substorm.



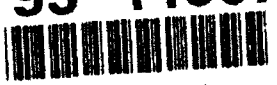

**14. SUBJECT TERMS**
DMSP, Ionosphere, Sub storm, Field-aligned currents

15. 22

**16. PRICE CODE**

| 17. SECURITY CLASSIFICATION OF REPORT | 18. SECURITY CLASSIFICATION OF THIS PAGE | 19. SECURITY CLASSIFICATION OF ABSTRACT | 20. LIMITATION OF ABSTRACT |
|---|---|---|---|
| UNCLASSIFIED | UNCLASSIFIED | UNCLASSIFIED | SAR |

*J. Geomag. Geoelectr.*, **45**, 1–22, 1993

# Characteristics of Suprathermal Electron Bursts Observed by the DMSP-F6/F7 Satellites in the Diffuse Aurora Region

H. NAKAJIMA[1], H. FUKUNISHI[1], T. ONO[2], and F. J. RICH[3]

[1]*Upper Atmosphere and Space Research Laboratory, Tohoku University, Sendai 980, Japan*
[2]*National Institute of Polar Research, Tokyo 173, Japan*
[3]*Phillips Laboratory, Geophysics Directorate, Hanscom AFB, MA 01731, U.S.A.*

(Received February 8, 1992; Revised September 16, 1992)

The particle data of the DMSP-F6 and -F7 satellites show the presence of suprathermal electron bursts in the diffuse aurora region. These bursts are characterized by intense (~$10^8$–$10^9$ (cm$^2$sr sec)$^{-1}$), low energy (~100–500 eV), and localized (~20–30 km at satellite altitude $h \simeq 830$ km) electron precipitation. Simultaneous magnetic field data from the DMSP-F7 satellite show that these bursts are often, but not always, accompanied with intense (few $\mu$Am$^{-2}$), small-scale (only few tens of km at satellite altitude) upward field-aligned currents. The bursts are observed from 19 h to 11 h MLT through midnight during the maximum to recovery phase of substorm. These bursts are less likely to be observed during geomagnetic storms than during times of isolated substorms. These results suggest that suprathermal electron bursts are generated by localized heating of ionospheric electrons which flow out from the ionosphere toward the magnetosphere during substorm.

## 1. Introduction

Suprathermal electron bursts have been observed by sounding rockets in a wide variety of auroral conditions. From two sounding rocket observations below 270 km altitude, RAITT and SOJKA (1977) reported that field-aligned suprathermal electron bursts occur with a duration of a few seconds and a peak energy in the range of 100–500 eV. Structured fluxes of 1 to 500-eV electrons found by DOERING *et al.* (1976) from the electron spectrometer experiment on the AE-C satellite are probably the same kind of electrons. Since the structured fluxes of electrons were frequently observed at all magnetic local times throughout the auroral region, DOERING *et al.* (1976) suggested that these low energy electrons must represent an important feature of the magnetosphere-ionosphere coupling system.

TANSKANEN *et al.* (1981) examined DMSP-F2 particle data and found the precipitation of low-energy electrons with fluxes exceeding $10^{10}$ (cm$^2$sr sec)$^{-1}$ near the equatorward boundary of the diffuse auroral region. These electrons appeared with a flux peak below 200 eV superimposed on hot electron population. TANSKANEN *et al.* (1981) interpreted these low energy electrons as part of an originally cold plasma, which was detached from the plasmasphere due to time-varying convective electric field and subsequently heated by the Landau damping of electromagnetic ion-cyclotron waves generated by hot, gradient-curvature drifting protons in the plasma sheet.

A detailed study of the suprathermal electron bursts was conducted by JOHNSTONE and WINNINGHAM (1982) using ISIS-2 soft particle spectrometer (SPS) data. They found that electron bursts occur both poleward and equatorward of discrete arcs but never within them. Electron bursts, which were observed for almost every pass across the nighttime auroral oval even during geomagnetically very quiet periods, were strongly field-aligned, usually confined to a pitch angle range less than 30°. The upper energy limit of bursts was less than the peak energy of the nearest arcs and decreased with distance from the arcs. From these results, JOHNSTONE and WINNINGHAM (1982) suggested that suprathermal electron bursts are an integral part of the main acceleration mechanism responsible for discrete arcs, and introduced an empirical model which accounts for the formation of suprathermal electron bursts and inverted-V events. Using both

DE-1 and DE-2 particle and wave data, ROBINSON *et al.* (1989) studied the plasma and field properties of suprathermal electron bursts. They found that suprathermal electron bursts are correlated with enhancements in the ac electric field at frequencies below 1 kHz, and concluded that electrons in suprathermal bursts are heated through interaction with waves, most likely ion cyclotron waves which are generated in regions of upward field-aligned currents and propagate obliquely away from the source region.

Counterstreaming electron beams discovered by SHARP *et al.* (1980) from the S3-3 satellite data at an altitude of ~1 $R_E$ are intense, narrowly collimated beams streaming simultaneously both parallel and antiparallel to magnetic field direction. These beams have characteristics similar to suprathermal electron bursts. The peak flux was $3 \times 10^{11}$ (cm$^2$sr sec keV)$^{-1}$ at an energy of 160 eV. LIN *et al.* (1982) observed two distinct types of counterstreaming electron events at altitudes of 2–3 $R_E$ with the High Altitude Plasma Instrument (HAPI) on the DE-1 satellite. Type 1 events are characterized by two Maxwellian distribution functions, an isotropic high-temperature component and a field-aligned low-temperature component, while type 2 events have only a field-aligned low-temperature component. Type 1 counterstreaming electrons are apparently the type of electron events reported by SHARP *et al.* (1980). COLLIN *et al.* (1982) studied the occurrence frequency, spatial distribution, and pitch angle distribution of upstreaming, downstreaming, and counterstreaming beams using the S3-3 satellite data of 181 polar passes. They showed that the beams are characterized by very soft (<400 eV) energy spectra and an extremely narrow pitch angle distribution with a median half width of 6°. In contrast, the peak fluxes had various values, sometimes exceeding $10^{11}$ (cm$^2$sr sec keV)$^{-1}$ although they were typically less than $3 \times 10^9$ (cm$^2$sr sec keV)$^{-1}$.

ARNOLDY *et al.* (1985) reviewed earlier measurements of field-aligned electrons, for which they used the term "FA electrons", including counterstreaming electrons. They, moreover, attempted further understanding the FA electrons by adding the University of New Hampshire rocket data. The upstreaming component of counterstreaming electrons was not observed at the low altitude level of the rocket, although downstreaming FA electrons were observed for 8 out of 10 evening auroral rocket flights. They concluded that FA electrons, whose spatial scales are tens of kilometers, are associated with evening, midnight, and cusp auroras, particularly, with active auroral forms on the edges of moving discrete arcs.

Using ground-based monochromatic CCD camera data and DMSP-F6 particle data, ONO *et al.* (1989) found that an east-west elongated auroral arc of OI 6300 Å emission appeared in correspondence with low-energy electron spikes observed by the DMSP-F6 satellite, and that the arc had a lifetime of more than few minutes. They concluded that the precipitation of such low energy electrons is intense enough to excite OI 6300 Å emissions but not OI 5577 Å emissions.

As reviewed above, suprathermal electron bursts (e.g., RAITT and SOJKA, 1977; JOHNSTONE and WINNINGHAM, 1982; ROBINSON *et al.*, 1989), "structured" flux of electrons (DOERING *et al.*, 1976), low energy electrons (TANSKANEN *et al.*, 1981), counterstreaming electrons (e.g., SHARP *et al.*, 1980; LIN *et al.*, 1982; COLLIN *et al.*, 1982), FA electrons (ARNOLDY *et al.*, 1985), and low energy electron spikes (ONO *et al.*, 1989) have a lot of common features. However, in former works attention has been focused mainly on the events associated with discrete auroras. In this paper, we investigate low energy electron bursts observed in the diffuse aurora regions using particle, magnetometer, and image data from the DMSP-F6 and -F7 satellites. Then the characteristics of selected burst events are compared with the former results. Since the peak energies of selected bursts are mostly between 100 and 500 eV, we hereafter use the term "suprathermal electron bursts" for representing them, although it is likely that they are not temporal "bursts", but rather small spatial structures as pointed out by ONO *et al.* (1989) and LU *et al.* (1991).

Although the particle detectors of the DMSP satellites observe only downward fluxes of precipitating electrons and ions, high resolution in time and energy (1 sec and 20 ch from 30 eV to 30 keV, respectively) and a wide coverage of the polar region by two satellites enable us to perform statistical study of suprathermal electron bursts in the diffuse aurora region. The magnetometer and image data simultaneously taken from the DMSP satellites are also useful for the study of the relationship among precipitating

particles, field-aligned currents, and visual auroras. In the present study, we picked out suprathermal electron burst events characterized by intense (~$10^8$–$10^9$ (cm$^2$sr sec)$^{-1}$), low energy (~100–500 eV), and localized (~20–30 km at satellite altitude of 830 km) precipitation in the diffuse aurora region. These events were observed at all local time sectors except the afternoon sector. Simultaneous DMSP-F7 magnetometer data showed that these electron precipitation events are often accompanied by intense (few $\mu$Am$^{-2}$), small-scale (only few tens of km at satellite altitude) upward field-aligned currents. The occurrence frequency of the events was closely related to substorm phase. A possible origin of suprathermal electron bursts in the diffuse aurora region is also discussed in this paper.

## 2. Satellite Instrumentation and Data Presentation

The DMSP (Defense Meteorological Satellite Program) F6 and F7 are three-axis stabilized satellites with an orbital period of 102 min and an altitude of 815–852 km. Both satellites have sun-synchronized orbits in the dawn-dusk (6:00–18:00 LT) meridian (F6) and in the noon-midnight (10:30–22:30 LT) meridian (F7). Although both satellites are sun-synchronized, they can cover a wide region in MLT-MLAT (magnetic local time-magnetic latitude) coordinates owing to the offset of the magnetic dipole axis from the earth's rotation axis. The common scientific instruments on F6 and F7 are an auroral scanner and a charged particle detector. The F7 satellite carries a magnetometer in addition to these instruments.

The charged particle detectors on board the F6 and F7 satellites are electrostatic analyzers called SSJ/4, which measure the fluxes of precipitating ions and electrons in the zenith direction (HARDY *et al.*, 1984). The fluxes are measured in 20 energy channels ranging from 30 eV to 30 keV. The time required to obtain one energy spectrum is 1 sec, which corresponds to 7.4 km at the satellite altitude and 6.6 km at the auroral emission height of 110 km.

Two dimensional auroral images are obtained by the auroral scanner using the forward motion of the satellite (EATHER, 1979). The spatial resolution of the auroral images is about 3.7 km at subtrack. The scanner has sensitivity in the spectral region of 4,000–11,000 Å, with a peak near 8,000 Å. The pitch and yaw errors of the scanner are less than 0.1°, which corresponds to 1.5 km on the altitude level of 110 km. The width of the auroral image is 2,958 ± 9 km.

The triaxial fluxgate magnetometer (code name, SSM) on board the DMSP-F7 satellite is a body-mounted magnetometer which measures the three components of ambient magnetic fields at a sampling rate of 20 vectors/sec by using a 13-bit A/D (analog to digital) converter (RICH, 1984). The range of the SSM is ±50,000 nT, and the one-bit resolution is 12 nT. Since the SSM is mounted at the satellite body, there is an offset of approximately 200 nT per axis. The three axes of the sensor unit are orthogonal within an accuracy of 0.1°.

The summary plots of DMSP particle and magnetometer data are presented in the format as shown in Fig. 1. This figure shows energy-time (E-T) diagram of precipitating ions (top panel) and total energy and number fluxes of precipitating ions (second panel), and those for precipitating electrons in the third and fourth panels, respectively. Time resolution of those data is 1 sec. In the E-T diagrams, corrected count number at each energy channel of the particle detectors is displayed in 10-step gray scale which is shown on the upper right hand side of the summary plot. Since the energy dependent geometric factor $G(E_i)$ derived from the calibration differs for each channel (HARDY *et al.*, 1984), the count number $N(i, t)$ at channel $i$ and time $t$ is normalized by the average geometric factor $\overline{G}$. Then the corrected count number $N_c(i, t)$ is given by $N_c(i, t) = N(i, t)\overline{G}/G(E_i)$.

Plotted in the fifth panel in Fig. 1 are the $Y$ and $Z$ components of magnetic field deviation from the model magnetic field which was calculated by the International Geomagnetic Reference Field (IGRF80) model. The directions of $Y$ and $Z$ are defined to be forward and horizontal, cross-track directions for the satellite, which are approximately north-south and east-west directions, respectively (see Fig. 1 in RICH, 1984). Small repetitive oscillations in the $Z$ component are probably due to an interference noise of the satellite.

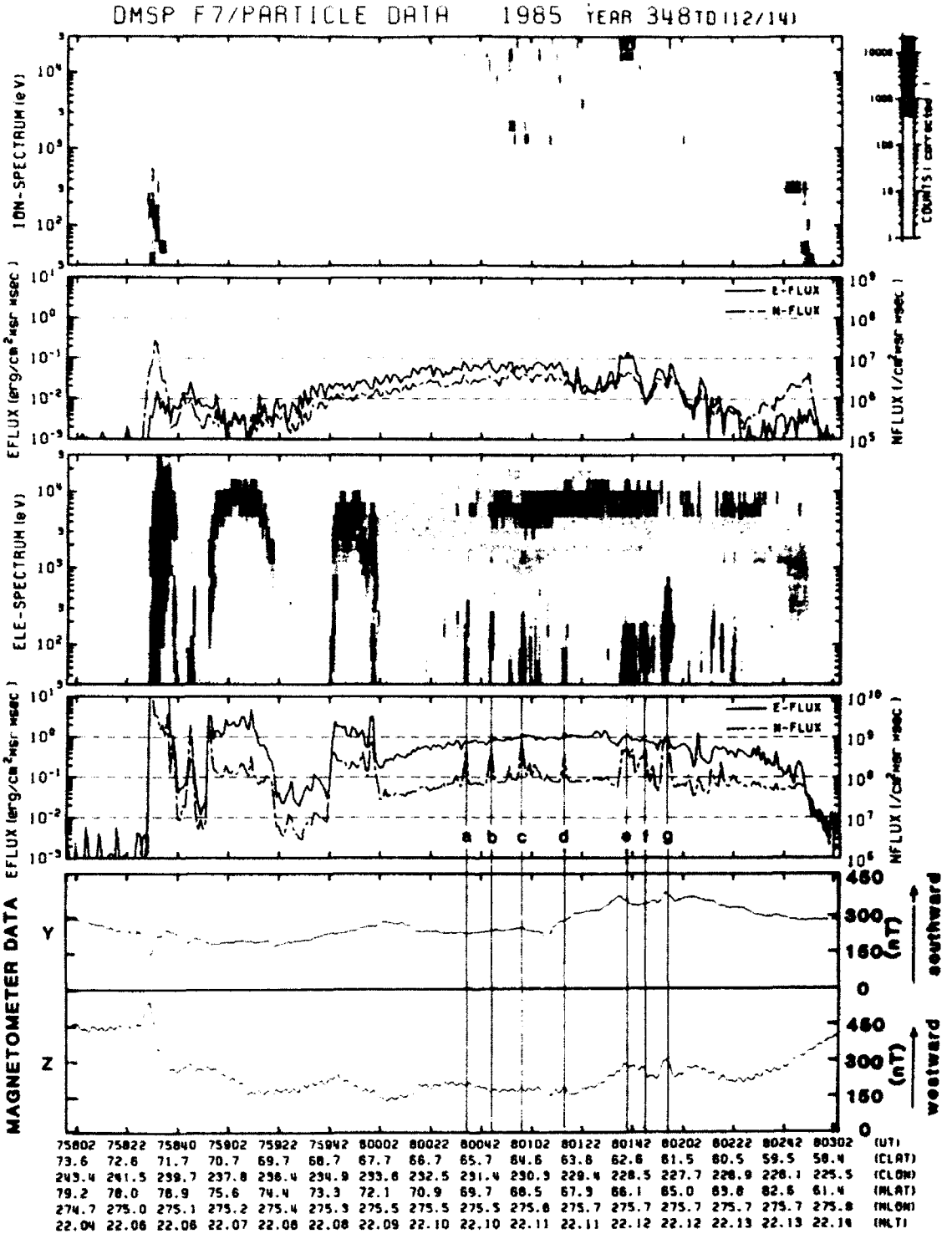


Fig. 1. Summary plot of the DMSP-F7 particle and magnetometer data in the time interval of 0758:02–0803:02 UT on December 14, 1985. The top and third panels show energy spectrograms of precipitating ions and electrons, respectively, while the second and fourth panels show total number fluxes and total energy fluxes of ions and electrons, respectively. The fifth panel shows the north-south and east-west components of magnetic perturbations. The orbital data of the satellite is given at the bottom. Vertical lines (a to g) represent suprathermal electron burst events.

## 3. Results

### *3.1 Selection of suprathermal electron burst events*

From the summary plots of the DMSP particle and magnetometer data described above, we can easily select suprathermal electron bursts. Figure 1 shows the summary plot of a DMSP-F7 northern polar pass from 0758:02 to 0803:02 UT, December 14, 1985. In general, the latitudinal profile of the auroral electron precipitation is divided into two regions, i.e., BPS (boundary plasma sheet) and CPS (central plasma sheet), which correspond to discrete and diffuse auroral regions, respectively (WINNINGHAM *et al.*, 1975). In the third panel of Fig. 1, BPS is found between 0758:30 and 0800:00 UT, in which a few inverted-V electron precipitation events are observed. CPS between 0800:00 and 0802:54 UT is characterized by diffuse electron precipitation with a broad peak between 5 to 10 keV. It is in this region that intense fluxes of suprathermal electron bursts are observed (see events a–g denoted by vertical lines in the fourth panel in Fig. 1).

In order to clearly show the relationship between the suprathermal electron bursts and auroras, we plotted the occurrence points of bursts on DMSP auroral scanner images. Figure 2 shows negative image of the DMSP scanning imager which was taken on the same pass as Fig. 1. The geographic coordinates at an altitude of 110 km, which are shown by solid lines at five degree intervals and dotted lines at one degree intervals, are superimposed on the image with an accuracy of ±1°. The orbit of the DMSP satellite is shown by a broken, horizontal line at the middle of the image, while the magnetic foot print of the DMSP satellite is shown by small dots near this line. The positions of suprathermal electron bursts are indicated

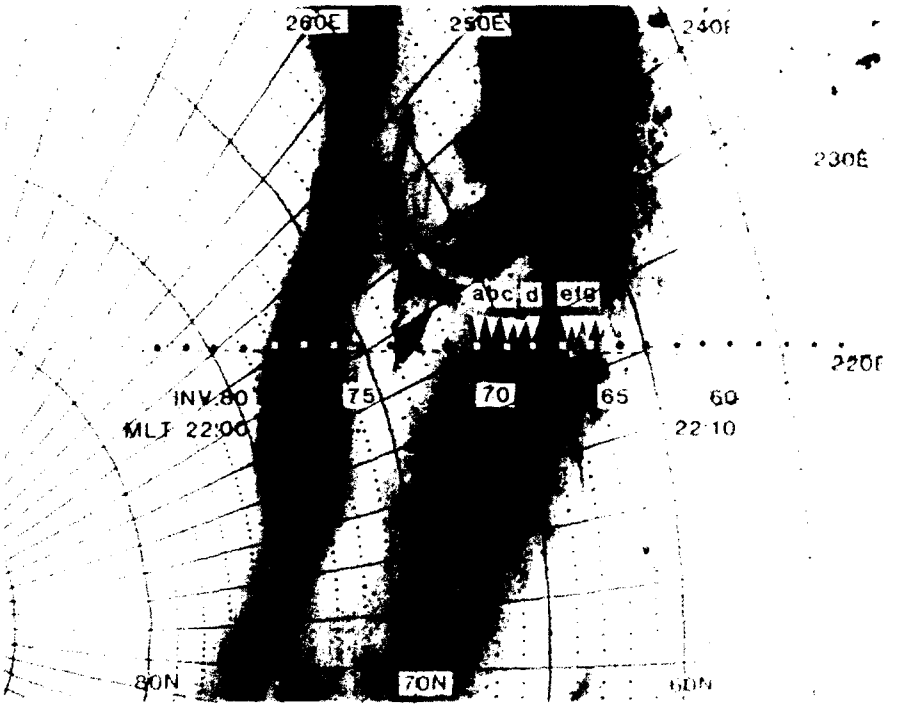


Fig. 2. A negative DMSP-F7 auroral scanner image taken between 0757:19 UT and 0805:51 UT on December 14, 1985. The location of suprathermal electron burst events is displayed on the image by triangles. The magnetic foot print of the DMSP-F7 satellite is represented by small dots in the vicinity of a broken horizontal line showing the center of the figure. The satellite passed from the left of the image to the right. The geographic coordinates are displayed by grids. The invariant latitude of the DMSP-F7 orbit is shown below the center line. This orbit is almost parallel to 22 h MLT meridian.

Table 1. Event number of suprathermal electron burst events.

| Satellite name | Period | total pass number | event number | pass number with event(s) | occurrence probability |
|---|---|---|---|---|---|
| DMSP-F6 | Sep.1–15, 1984 | 422 | 85 | 40 | 9.5% |
| DMSP-F7 | Sep.1–15, 1984 | 422 | 180 | 64 | 15.2% |
| Total | | 844 | 265 | 104 | 12.3% |

by triangles.

By comparing Fig. 2 with Fig. 1, it is obvious that inverted-V events observed around 0759:10 and 0759:50 UT, and an intense precipitation event at the poleward edge (0758:34 UT) corresponds to discrete auroras, while suprathermal electron bursts occurred in the diffuse aurora region located equatorward of discrete auroras. No visible auroral features are seen in Fig. 2 corresponding to suprathermal electron bursts.

We have selected suprathermal electron bursts from the DMSP particle data. The data period in the present analysis is September 1–15, 1984 for both DMSP-F6 and DMSP-F7. We limited the sampling area of suprathermal electron burst events within the diffuse aurora region characterized by diffuse, high energy (~1–10 keV) electron precipitation according to the reason presented in the discussion. We also selected events with a criterion that the total number flux inside of each event is five times larger than the precipitating electron fluxes outside of event. The total number of events selected is 265 as shown in Table 1. The number of DMSP passes with single or multiple suprathermal electron burst events in the diffuse aurora region and its percentage to the total pass number are also shown in Table 1.

### *3.2 Statistical characteristics of suprathermal electron bursts*

Using the 265 suprathermal electron bursts selected, we examined the distributions of energy at maximum number flux, total number flux, and duration time. First, the distribution of energy at maximum number flux is shown in Fig. 3 as a function of the SSJ/4 energy channel. It is obvious that 94% events have flux peaks between ch.3 (65 eV) and ch.9 (646 eV). These energy ranges are similar to those in former studies (e.g., DOERING *et al.*, 1976; SHARP *et al.*, 1980; JOHNSTONE and WINNINGHAM, 1982; COLLIN *et al.*, 1982). Note that these energy ranges are much higher than those of ionospheric electrons and lower than those of hot plasma sheet electrons. The statistical result on number flux of suprathermal electron bursts is presented in Fig. 4. Here, we used the total number flux *JTOT* given by the equations;

$$JTOT = \sum_i J(E_i) \frac{E_{i-1} - E_{i+1}}{2}, \tag{1}$$

$$J(E_i) = \frac{C_i / \Delta T}{G(E_i)}, \tag{2}$$

where $J(E_i)$ and $C_i$ denote the differential number flux for each energy channel with the central energy $E_i$ and the number of counts of each channel, respectively, while $G(E_i)$ and $\Delta T$ denote the energy dependent geometric factor for channel $i$ and the accumulation time which is equal to 98 milliseconds, respectively. The contribution of the diffuse precipitation of high energy electrons to *JTOT* is usually less than one fifth of the total value. Figure 4 shows that the values of total number flux are widely distributed between $1 \times 10^8$ and $2 \times 10^9$ (cm$^2$sr sec)$^{-1}$. These values are much larger than those of ambient, diffuse precipitation of 1–10 keV auroral electrons, but smaller than the result of TANSKANEN *et al.* (1981). It is also found that the total number flux of suprathermal electron bursts in the diffuse aurora region is almost equal to that

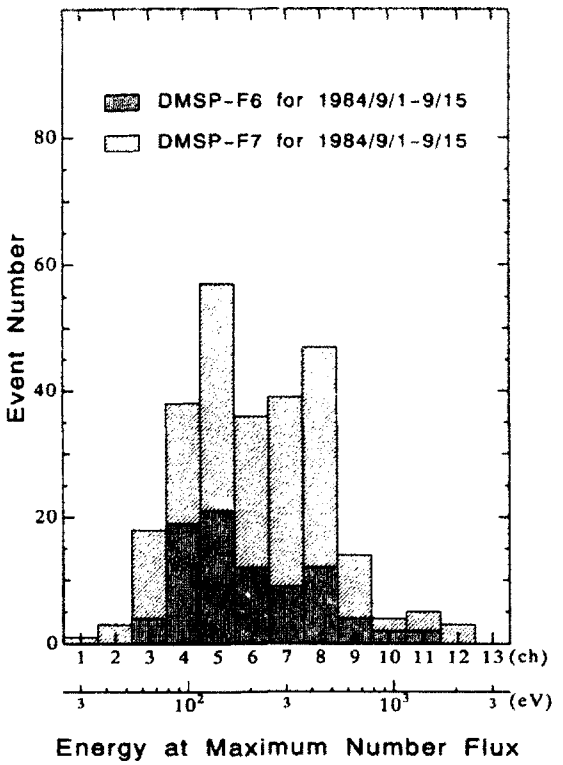


Fig. 3. Distribution of energy at maximum number flux for 265 suprathermal electron burst events selected from the DMSP-F6 and -F7 particle data in the periods of September 1 to 15, 1984.

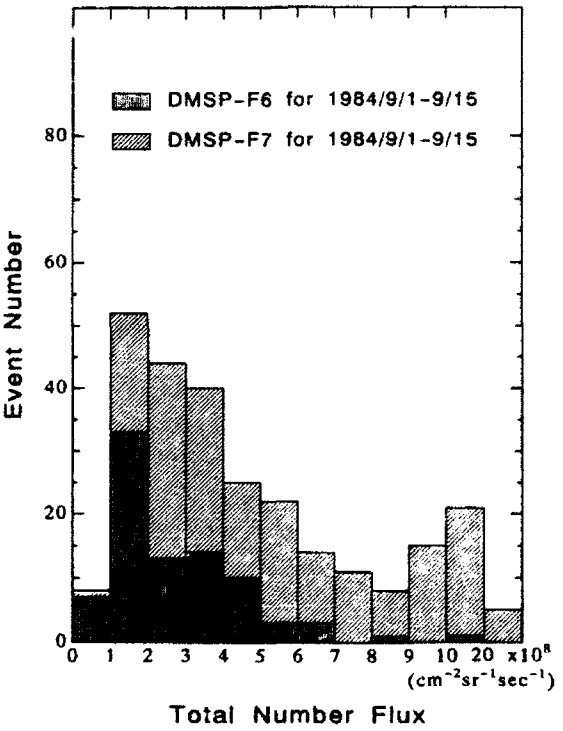




Fig. 4. Distribution of total number flux for 265 suprathermal electron burst events selected from the DMSP-F6 and -F7 particle data in the period of September 1 to 15, 1984.

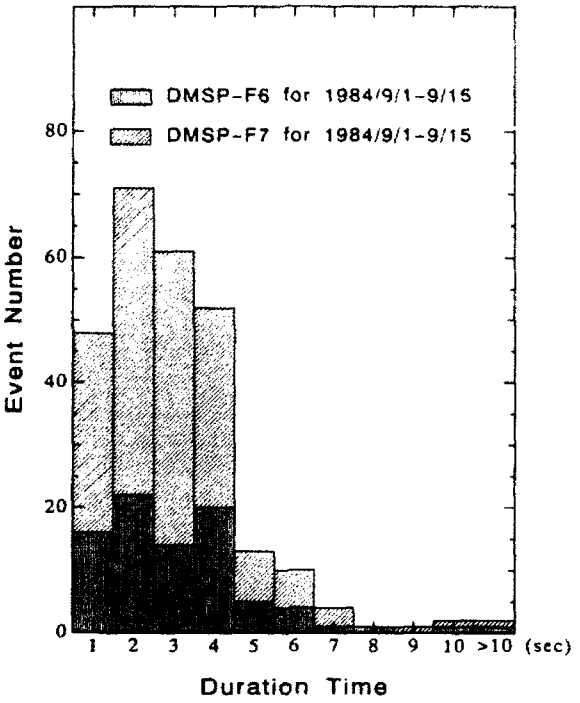


Fig. 5. Distribution of duration time for 265 suprathermal electron burst events selected from the DMSP-F6 and -F7 particle data in the period of September 1 to 15, 1984.

of inverted-V electrons.

The statistical result on the duration time of bursts is shown in Fig. 5. It is apparent that 88% bursts have duration time shorter than 5 sec. This value corresponds to 37 km at the satellite altitude ($h \simeq 830$ km) since the orbital velocity of the satellite is 7.4 km/sec. It also corresponds to 25 km at the auroral emission height ($h \simeq 110$ km) at 70° in magnetic latitude. Previous results (e.g., JOHNSTONE and WINNINGHAM, 1982; ARNOLDY *et al.*, 1985; ONO *et al.*, 1989) showed similar spatial scale of tens of kilometers at satellite and rocket altitudes. It is important to note that suprathermal electron bursts are localized in such narrow regions in latitude.

### *3.3 Occurrence region of suprathermal electron bursts*

The occurrence region of 265 bursts selected from the DMSP-F6 and -F7 particle data in the period from September 1 to 15 in 1984 are plotted in MLAT-MLT plane in Fig. 6. The orbits of the DMSP-F6 and -F7 satellites for September 1, 1984 and the mean auroral oval are also plotted in Fig. 7. Those figures show following characteristics:

(i) Suprathermal electron bursts are observed in the magnetic local time sector from 19 h to 1 h and from 3 h to 11 h. Since a gap of occurrence between 1 h and 3 h MLT could be due to an incomplete coverage of DMSP orbits as is shown in Fig. 7 and by shaded areas in Fig. 6, it is likely that bursts occur in the crescent area at magnetic local time sector from 19 h to 11 h MLT through midnight.

(ii) Suprathermal electron bursts occur in the region from 60° to 70° MLAT (corrected magnetic latitude) for the evening to morning sector (19 h–5 h MLT) and in the region from 65° to 75° MLAT for the morning to noon sector (5 h–11 h MLT).

The crescent shaped occurrence region of suprathermal electron bursts is very similar to the intense electron precipitation region on the maps of total energy flux given by HARDY *et al.* (1985) for $Kp = 3$ to 5. The difference between the spatial distribution given in Fig. 6 and the spatial distributions of other low energy electron precipitation events given by DOERING *et al.* (1976), JOHNSTONE and WINNINGHAM

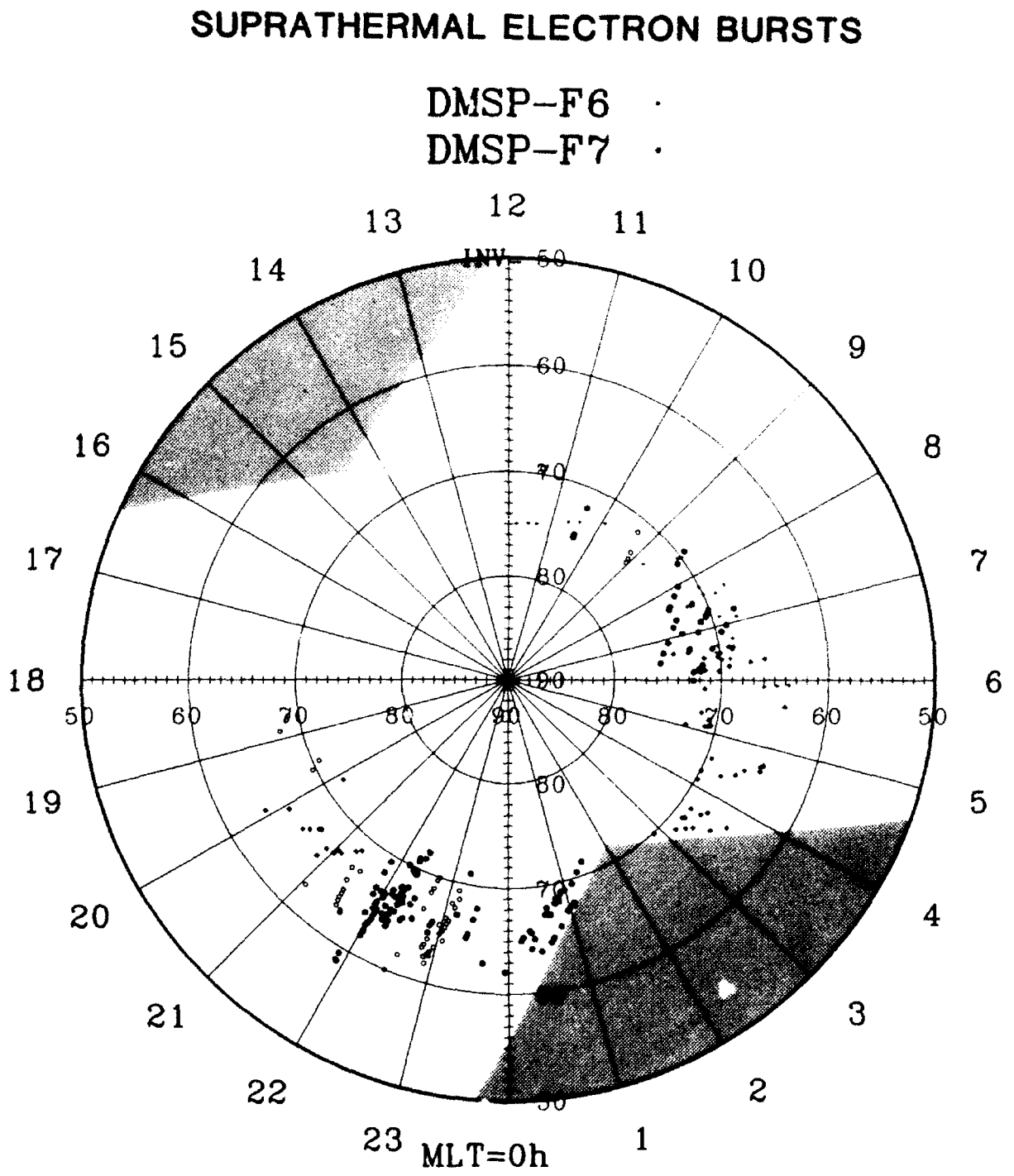


Fig. 6. Spatial occurrence map of 265 suprathermal electron burst events in MLAT-MLT coordinates. These events were observed for 15 days from September 1 to 15, 1984 by the DMSP-F6 and -F7 satellites. Crosses and open circles represent suprathermal electron burst events observed by the DMSP-F6 and -F7 satellites, respectively. Thick crosses and circles indicate the events observed on north pole passes, while thin crosses and circles indicate those observed on south pole passes. Shaded areas represent the gaps of orbital coverage of the DMSP-F6 and -F7 satellites.

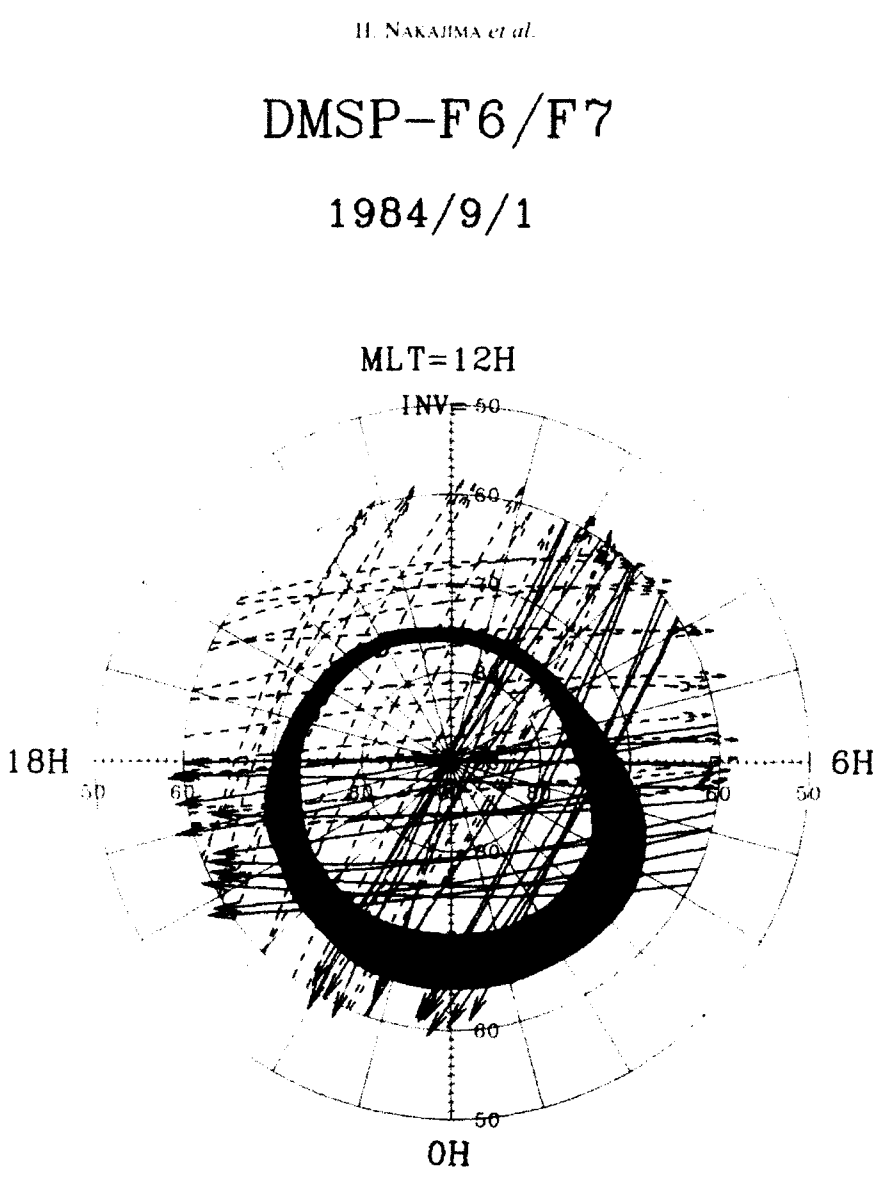


Fig. 7. DMSP-F6 and -F7 orbits for September 1, 1984 in MLAT-MLT plane. The F6 satellite has dawn-dusk (6:00-18:00 LT) orbits, while the F7 satellite has noon-midnight (10:30-22:30 LT) orbits. Solid arrows represent the north polar passes, while broken arrows represent the south polar passes. Both satellites revolve around the earth 14 times a day. The mean auroral oval (Fig. 2 in FELDSTEIN, 1966) is also represented by shaded area.

(1982), and COLLIN *et al.* (1982) is discussed later.

Figure 8 shows the relationship between the diffuse aurora region decided by the DMSP particle data and the occurrence region of suprathermal electron bursts. The locations of both regions are represented on orbits in the MLT-MLAT plane by thin broken and thick continuous lines, respectively. The size of open circles at both ends of each orbit in Fig. 8 shows *Kp*-indices at times when suprathermal electron burst events were observed. The relation between the size of open circles and the corresponding *Kp* values is given on the right-hand side. In this figure, it is found that suprathermal electron bursts occur mostly in the midst, not near the poleward boundary of the diffuse aurora region. It is also found that the diffuse aurora and electron burst regions expands equatorward with increasing *Kp* value. The equatorward expansion of the diffuse aurora boundary according to *Kp* values agrees with the result of GUSSENHOVEN *et al.* (1983).

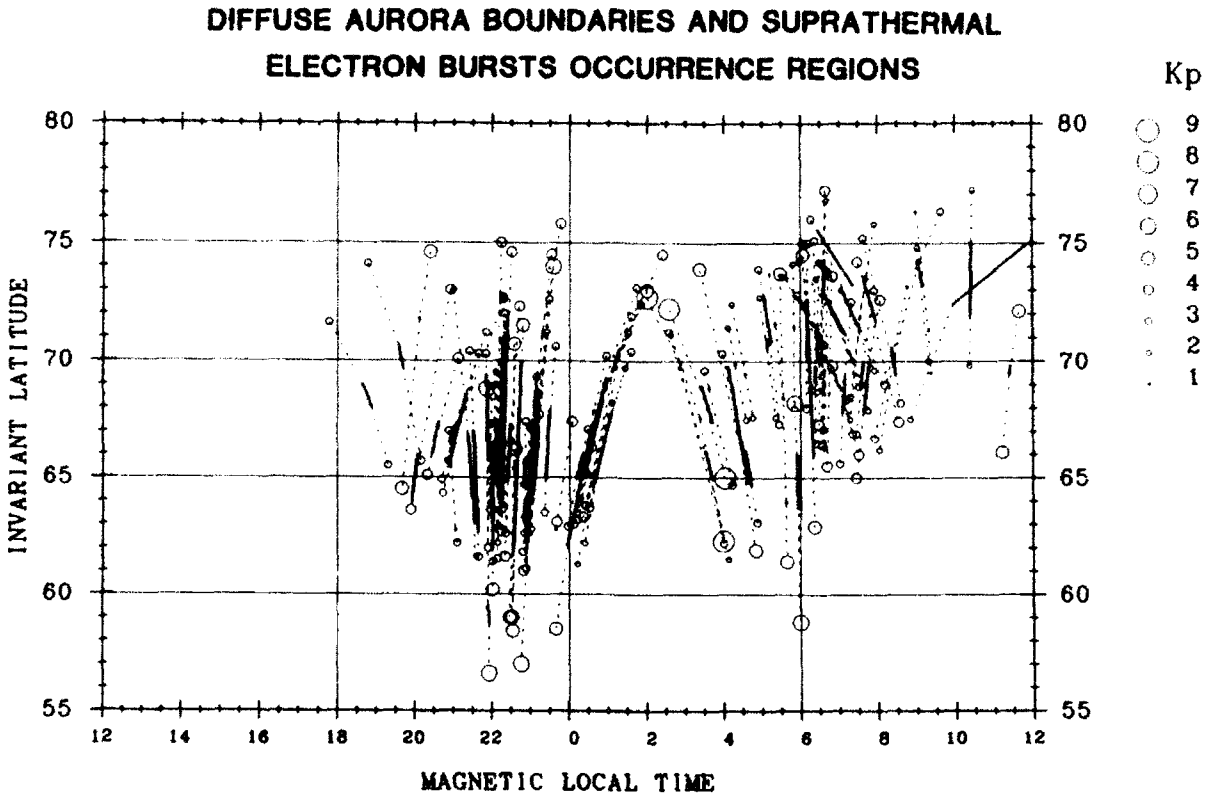


Fig. 8. Spatial relationship between the diffuse aurora region and the occurrence region of suprathermal electron bursts in MLAT-MLT coordinates. The data period is the same as that in Fig. 6. The diffuse aurora region defined from the DMSP particle data is shown by broken lines, while the occurrence region of suprathermal electron bursts is shown by thick lines along DMSP orbits. The size of open circles at both ends of each orbit indicates *Kp*-value at times when suprathermal electron burst events were observed.

### *3.4 Dependence on substorm activity*

The dependence of suprathermal electron bursts on substorm activity is very important to study the generation mechanism of suprathermal electron bursts in the diffuse aurora region. First, we have examined the dependence of suprathermal electron bursts on *Kp*-index for 15 days in the periods of September 1–15, 1984. The result is shown in Fig. 9, in which bursts are found to occur more frequently in geomagnetically disturbed periods than in quiet periods with the occurrence probability of 93% for $Kp \geq 2$. The probability for $Kp \geq 2$ in this data period is 83%. The mean value of *Kp*-index for the period when bursts occurred is 3.2, while the average *Kp* value during the whole data period analyzed is 2.9. Since there exist times for even $Kp \geq 4$ when no suprathermal electron bursts are observed, it is likely that these bursts are associated with isolated substorms rather than with geomagnetic storms.

Although *Kp*-index is a good indicator of magnetic activity, we can not discuss the dependence of suprathermal electron burst events on substorm phase using *Kp*-index, since individual substorms have a time scale of ~1–3 hours which is shorter than the time resolution of *Kp*-index. As a next step, we have examined the relationship between the substorm phase and occurrences of bursts using auroral electrojet (*AE*) index. Figure 10 shows, in the magnetic local time versus *AE*-index plane, the number of pass in which bursts occurred. This statistical result was obtained from DMSP-F6 and -F7 data in the period of September 1–15, 1984. It is found that bursts occur for various values of *AE*-index ranging from 0 to 800 nT, and in the local time sector from 20 h to 11 h MLT. Although it seems that bursts have their occurrence peaks around 22 h and 7 h MLT, the true occurrence peak is unknown since the number of DMSP pass

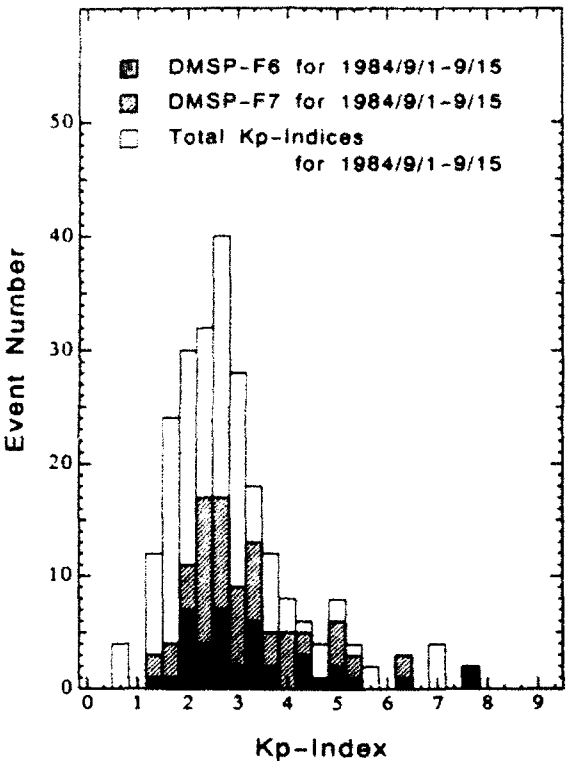


Fig. 9. *Kp* dependence of 256 suprathermal electron burst events observed on the DMSP-F6 and -F7 satellites for 15 days from September 1 to 15, 1984. Shaded columns represent the number of passes when bursts are observed, while open columns represent the distribution of *Kp*-values for the whole period analyzed. The height of open columns are doubled in order to compare them with shaded ones.

is few in 3 h to 5 h MLT and none around 2 h MLT at the magnetic latitude of the diffuse aurora region as shown in Fig. 7. The most noteworthy feature in Fig. 10 is that *AE*-index at times when bursts occurred have a maximum around 22 h MLT and decrease toward morning hours. If suprathermal electron bursts occur simultaneously in the whole MLT region, these bursts should be equally distributed in the *AE*-MLT plane. Judging from this tendency, we suggest that occurrence region of bursts shifts toward the dawn side as the substorm activity declines.

However, there is some limitation for further interpretation of Fig. 10 because the DMSP satellites have an orbital period of 102 min, and therefore bursts found in the DMSP particle data are snapshots of the whole events. Here, we try another approach to determine the substorm phase using *AE*-index.

Although the temporal variation of *AE*-index is fairly complex, it is possible to classify the temporal variation pattern of *AE*-index into five phases (A to E). Figure 11 shows a schematic diagram defining the five phases and an example of a sequence of *AE*-index classified by this definition. Phase A is a quiet time before the substorm, and phase B is the first expansion phase, while phase C is the recovery phase. When there are successive occurrences of substorms, we alternatively define phase D for the expansion phase and phase C for the recovery phase. When the substorm finally declines, phase E is defined to be the period when *AE* index value becomes less than 100 nT. After one hour interval of phase E, next phase A starts. Using this classification, the *AE*-MLT diagram presented in Fig. 10 was classified into the five phases, as shown in Fig. 12. It is apparent that there is no event in phase A, and that only two events occur in phase B. The most frequent occurrence of suprathermal electron bursts is seen in phase C, the next frequent occurrence in phase D, and the occurrence number decreases in phase E. Moreover, it is found that bursts in phase E occur only in the dawn sector from 4 h to 10 h MLT. Although the total time period of each

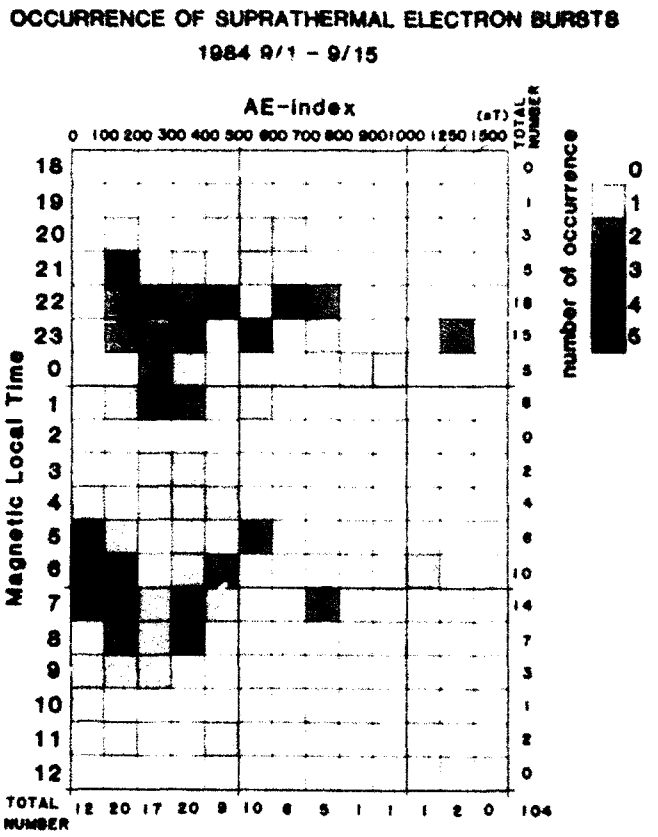


Fig. 10. *AE*-MLT plots of 104 passes when suprathermal electron bursts are observed on the DMSP-F6 and -F7 satellites for 15 days from September 1 to 15, 1984. The axis of ordinates represents magnetic local time at one-hour intervals, e.g., 6 h MLT represents the time span between 0530 and 0629 MLT. The local time sector between 12 h and 18 h MLT is not shown in this figure because there is no suprathermal electron burst event in this region. Total occurrence number for each division of MLT and *AE* ranges is given on the right and at the bottom of the figure, respectively.

phase is not equal, these results suggest that suprathermal electron bursts occur most frequently at the maximum to recovery phase of single or multiple substorms.

The time scale of the duration of bursts around 22 h MLT region can be estimated when we carefully examine Fig. 12. Since there is no event in phase E in the 20 h–1 h MLT sector, which is considered to be the initial occurrence region of bursts due to the reason mentioned before, the duration of burst events in this local time sector appears to be less than one orbital period (~100 min) of the DMSP satellites according to the following reason. If suprathermal electron bursts last over one orbital period of the DMSP satellites, there would be an opportunity to observe bursts on geomagnetic conditions corresponding to phase E since the values of *AE*-index often decreases to less than 100 nT within one orbital period.

The features of suprathermal electron bursts concerning the dependence on substorm phase are summarized as follows:

(i) These bursts occur mainly in the maximum to recovery phase of substorms, and rarely in the early expansion phase. There is no occurrence of bursts on quiet time before substorms.

(ii) As the substorm activity declines, the burst occurrence region shifts towards the dawn side, reaching the 4–11 h MLT sector when the intensity of *AE*-index decreases below 100 nT.

(iii) The duration of the bursts around 22 h MLT is estimated to be less than one orbital period (~100 min) of the DMSP satellite.

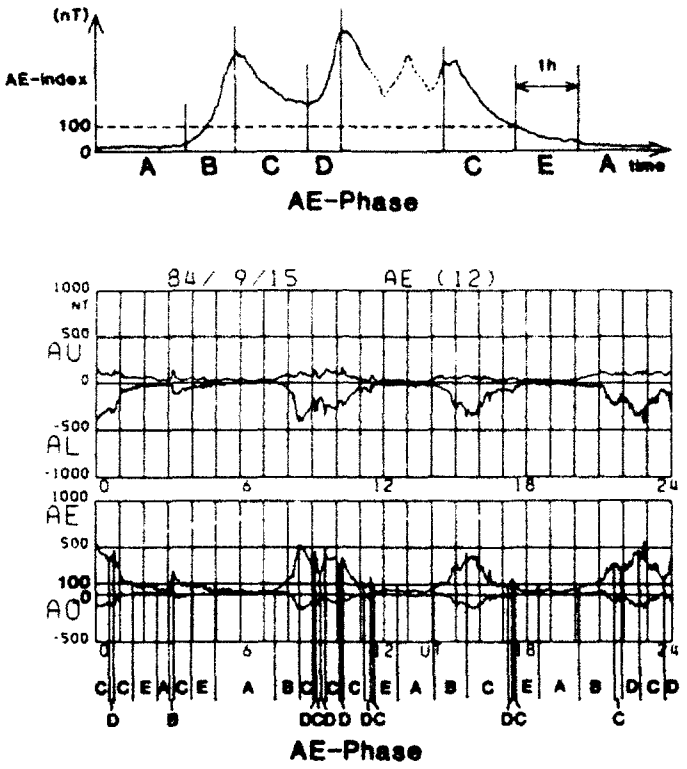


Fig. 11. Schematic diagram showing a classification of substorm phase and an example of *AE*-index sequence classified into six categories. Substorm phase is classified into six categories—A to E. A is the quiet phase, B is the first expansion phase, C is the recovery phase, D is the second or successive expansion phase of multiple substorms, and E is the post substorm phase. When multiple onsets of substorm occur, C-D pairs repeat. Bottom panel represents the traces of *AU*, *AL*, and *AE*-indices on September 15, 1984.

### *3.5 Small-scale field-aligned currents associated with suprathermal electron bursts*

The relationship between suprathermal electron bursts in the diffuse aurora region and field-aligned currents (FACs) have been examined using the magnetometer data of the DMSP-F7 satellite. Large-scale field-aligned currents which connect the ionosphere and the magnetosphere are concentrated into two principal areas encircling the geomagnetic pole. These field-aligned current flow regions have been designated by IIJIMA and POTEMRA (1976) as "region 1" and "region 2" located at the poleward and equatorward sides, respectively. During geomagnetically disturbed period, the field-aligned current region expands and shifts to lower latitude, but the basic flow pattern of region 1 and region 2 currents remains unchanged. The densities of region 1 and region 2 currents are not necessarily equal at given local time.

In Fig. 1, we have presented the summary plot of DMSP-F7 particle and magnetometer data for the time interval of 0758:02–0803:02 UT on December 14, 1985. The magnetic local time of this orbit is 22 h, and the diffuse aurora region extends from 71.4° to 61.9° MLAT where many suprathermal electron bursts occur. The *AE*-index sequence on December 14, 1985, which is shown in Fig. 13, suggests that this event occurred in the recovery phase of a small substorm. There are seven bursts which meet the criteria for selection of suprathermal electron bursts. The occurrence times of these seven bursts, which are designated as a to g, are displayed by vertical lines in Fig. 1. The most intense burst event (event g) occurred in 0801:54–0801:57 UT. Just corresponding to this event, an impulsive magnetic variation is seen both in the $Z$ and $Y$ components of magnetic perturbations. The amplitude and direction of the

| MLT (h) | 0 | 100 | 200 | 300 | 400 | 500 | 600 | 700 | 800 | 900 | 1000 | 1250 | 1500 < (nT) | TOTAL |
|---|---|---|---|---|---|---|---|---|---|---|---|---|---|---|
| 18 | | | | | | | | | | | | | | 0 |
| 19 | | | | | | C | | | | | | | | C=1 1 |
| 20 | | | C | | | | C | | D | | | | | C=2 D=1 3 |
| 21 | | | CC D | | C | | C | | | | | | | C=4 D=1 5 |
| 22 | | | C D | CC CC | C D | CC D | | CC C DD | C D | | | | | C=12 D=6 18 |
| 23 | | | B D | C D | CC D | | CC CC D | | C | | | | CC | B=1 C=10 D=4 15 |
| 0 | | | | CC | D | | | | | C | C | | | C=4 D=1 5 |
| 1 | | | C | B CC C | C D | | C | | | | | | | B=1 C=6 D=1 8 |
| 2 | | | | | | | | | | | | | | 0 |
| 3 | | | | C | C | | | | | | | | | C=2 2 |
| 4 | E | | | C | C | D | | | | | | | | C=2 D=1 E=1 4 |
| 5 | EE | | C | | C | | C D | | | | | | | C=3 D=1 E=2 6 |
| 6 | EE EE | | CC | | C | DD | | | | | | C | | C=4 D=2 E=4 10 |
| 7 | E EE | | CC C D | C | CC C | D | | | DD | | | | | C=7 D=4 E=3 14 |
| 8 | | | CC | C | CC C D | | | | | | | | | C=6 D=1 7 |
| 9 | E | | D | D | | | | | | | | | | D=2 E=1 3 |
| 10 | E | | | | | | | | | | | | | E=1 1 |
| 11 | | | C | | | C | | | | | | | | C=2 2 |
| 12 | | | | | | | | | | | | | | 0 |
| TOTAL | E=12 12 | | B=1 C=14 D=5 20 | B=1 C=14 D=2 17 | C=15 D=5 20 | C=4 D=5 9 | C=8 D=2 10 | C=3 D=3 8 | C=2 D=3 5 | C=1 1 | C=1 1 | C=1 1 | C=2 2 | 0 | B=2 C=65 D=25 E=12 104 |

Fig. 12. Substorm phase (A–E defined in Fig. 11) dependence of 104 passes in which suprathermal electron bursts are observed on the DMSP-F6 and -F7 satellites for 15 days from September 1 to 15, 1984. The definition of horizontal and vertical divisions is the same as defined in Fig. 11. Event number for each group is also given at the right and bottom of the figure.

variation are 72 nT and eastward for the $Z$ component ($DBz$), and 41 nT and northward for the $Y$ component ($DBy$), respectively. This type of magnetic variation can be produced when the satellite passes through an upward field-aligned current sheet from poleward to equatorward. The amplitude of total horizontal perturbations $DBh$ is calculated by

$$DBh = \sqrt{DBz^2 + DBy^2}. \tag{3}$$

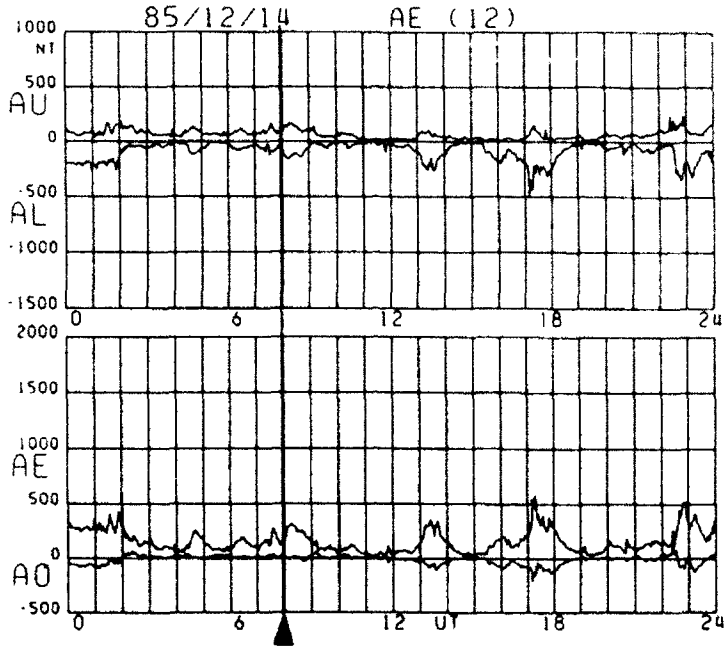


Fig. 13. Top panel shows *AU* and *AL* indices, while bottom panel shows *AE* and *AO* indices of December 14, 1985. A thick vertical line near 0800 UT represents the time when the DMSP-F7 satellite observed suprathermal electron bursts.

For the case of event g, *DBh* is equal to 83 nT, which corresponds to an upward current density of 3.0 $\mu Am^{-2}$ if the satellite orbit crosses perpendicular to a current sheet with a width of 3 sec in flight time (3 sec $\simeq$ 22 km at $h$ = 830 km). A procedure for the estimation of current density and current intensity from the magnetometer data is described in Appendix. In the case of much larger *Z* component perturbation than *Y*, approximate intensity of field-aligned current can be estimated from only *Z* component perturbation by assuming an infinite east-west elongated current sheet.

Though the luminosity of aurora is mainly controlled by high energy ($\geq$1 keV) particles (mainly electrons), filed-aligned current density is determined by total number flux of precipitating/upgoing particles. Since the mobility of electrons is much higher than that of ions in the magnetosphere, electrons mainly contribute to field-aligned current density. Assuming an isotropic pitch angle distribution for downward electrons, the current intensity is estimated at 4.1 $\mu Am^{-2}$ for total number flux of event g ($1 \times 10^9$ $(cm^2 sr\ sec)^{-1}$). Since this value is close to the value deduced from magnetometer data (3.0 $\mu Am^{-2}$), suprathermal electron bursts may be the main current carrier of intense, small-scale field-aligned currents appeared in the large-scale "region 2" field-aligned current system. However, we can not precisely evaluate the contribution of these suprathermal electrons on small-scale field-aligned currents, since the DMSP-F7 satellite measures only downward particle fluxes. If the pitch angle distribution of suprathermal electrons is more collimated along magnetic field lines, the current density inferred from the total number flux is over estimated. If we assume that the downward electron beam is confined within 30°, the calculated current intensity becomes 1.3 $\mu Am^{-2}$. Actually, sharply collimated suprathermal electrons named "counterstreaming electrons" were reported by rocket and DE-1 satellite observations (SHARP *et al.*, 1980; LIN *et al.*, 1982; COLLIN *et al.*, 1982).

Another interesting feature in Fig. 1 is that westward deviation in the *Z* component perturbation is seen at the poleward side of event g. The westward deviation is 80 nT, which corresponds to a downward field-aligned current of 2.9 $\mu Am^{-2}$ for a latitudinal scale of 3 sec (~22 km at $h$ = 830 km). In the vicinity of events e and f, we observe again a small scale ($\leq$50 km at $h$ = 830 km) upward and downward field-

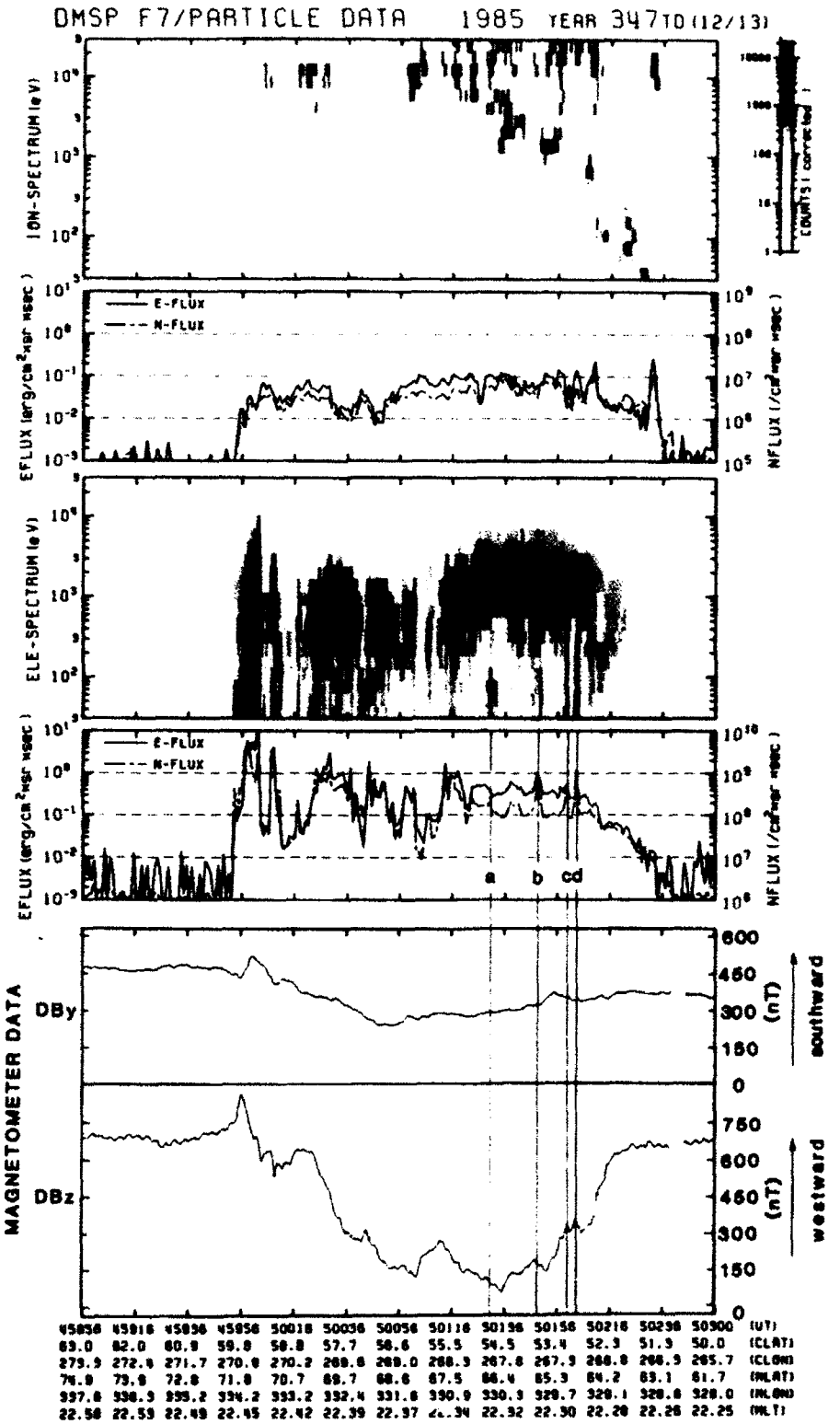


Fig. 14. Summary plot of the DMSP-F7 particle and magnetometer data from 0458:56 to 0503:00 UT on December 13, 1985. The notation is the same as that in Fig. 1. Vertical lines a to d represent suprathermal electron burst events.

aligned current pair. Since downward currents are frequently observed in the vicinity of upward currents corresponding to suprathermal electron bursts, these downward currents are suggested to be the return currents of the upward currents. Since there is no particular precipitation of electrons and ions in the downward current region, a possible candidate for the current carrier appears to be ionospheric cold electrons which flow out from the ionosphere to the magnetosphere. At event d, upward, but not so strong, field-aligned current is also seen on the *DBz* component. However, upward currents are scarcely seen at events a, b, and c.

The close relationship between suprathermal electron bursts and small-scale field-aligned currents is demonstrated again in Fig. 14 for 0458:56–0530:00 UT on December 13, 1985. Four bursts (a to d) are found in the diffuse electron precipitation region. This pass corresponds to the recovery phase of a substorm. The DMSP-F7 satellite traversed the northern hemisphere premidnight sector from north to south. The magnetometer data show the presence of typical upward region 1 FAC's poleward and downward region 2 FACs equatorward. It is found that four suprathermal electron bursts occurred in the region 2 FAC region. At the times of events a to d, small-scale magnetic variations with a duration time of ~2 sec and a magnitude between 20 to 50 nT were observed only in the *DBz* component. These magnetic perturbations correspond to 1.2 to 3.0 $\mu Am^{-2}$ in current density when we assume that they are not temporal but spatial structures.

### *3.6 Summary of the characteristics of suprathermal electron bursts*

As we have shown above, it has become clear that the suprathermal electron bursts have following features:

(i) They occur in the diffuse aurora region located in the equatorward part of the auroral oval.

(ii) The energy of precipitating electrons is mostly less than 500 eV.

(iii) Total number flux is $\sim 10^8$–$10^9$ $(cm^2 sr\ sec)^{-1}$, which is comparable with that of inverted-V's.

(iv) Assuming that these bursts are not temporal bursts but rather spatial structures, the latitudinal width of the bursts is usually less than 30 km at the auroral emission height of 110 km.

(v) The bursts tend to occur in geomagnetically disturbed periods with *Kp*-index larger than 2.

(vi) The bursts are often accompanied by intense (few $\mu Am^{-2}$), small-scale field-aligned currents.

## 4. Discussions

The low energy electron precipitation events investigated in former works and the suprathermal electron bursts in the diffuse aurora region presented in this paper have many common characteristics concerning energy at maximum number flux, total number flux, and spatial scale. Therefore, we discuss these characteristics in comparison with former works.

In the present paper, it has been found that suprathermal electron bursts occur in the central part of the diffuse aurora region and in the magnetic local time sector from 19 h to 11 h MLT except the afternoon sector. This local time sector corresponds to the region with population of electrons injected from the night-side plasma sheet (SANDAHL and LINDQVIST, 1990). DOERING *et al.* (1976) studied the spatial distribution of "structured" electron fluxes in northern high-latitude region using AE-C satellite data, and concluded that "structured" fluxes occur at all local times in the auroral oval. However, when we carefully examine the result of DOERING *et al.* (1976), it is found that the "structured" fluxes in the early afternoon hours was observed only in disturbed ($Kp \geq 3$) period. Therefore, it is likely that cusp precipitation events around noon are included in their occurrence map.

The spatial distribution of counterstreaming electrons was reported by COLLIN *et al.* (1982) using S3-3 satellite data. It was shown that the spatial distribution has two peaks, one at ~7 h MLT in the morning sector and another at ~22 h MLT in the evening sector. This result seems to be consistent with the result presented in Fig. 10, although the true occurrence peak is unknown due to an incomplete coverage of the DMSP satellites in our case. As mentioned in the previous section, the crescent shaped occurrence region of suprathermal electron bursts is very similar to the intense electron precipitation region on the maps of

total energy flux given by HARDY *et al.* (1985) for $Kp = 3$ to 5. This result implies that the source region of the bursts is the Central Plasma Sheet.

JOHNSTONE and WINNINGHAM (1982) observed suprathermal electron bursts both poleward and equatorward of discrete arcs for almost every pass of the ISIS-2 satellite. In our study, we omitted low energy electron precipitation events occurred poleward of discrete arcs because; 1) the occurrence frequency of suprathermal electron bursts poleward of discrete arcs is much less than that of equatorward events, and 2) it is not easy to distinguish poleward precipitation events from cusp precipitation events. JOHNSTONE and WINNINGHAM (1982) regarded the suprathermal electron bursts as an integral part of the main acceleration mechanism responsible for discrete arcs, since burst events are observed even during quiet period. However, it was shown in this paper that suprathermal electron bursts in the diffuse aurora region occur only in disturbed time.

DOERING *et al.* (1976) showed the difference in spatial distributions of "structured" electron flux events during quiet and disturbed periods. HOFFMAN *et al.* (1985) examined the occurrences of suprathermal electron bursts for three geomagnetic activity levels, i.e., quiet, substorm onset, expansion, and recovery levels using ground magnetometer data. Bursts were observed for onset and recovery levels, while any bursts were not observed during quiet times. In this paper, it has been revealed that suprathermal electron bursts occur mostly in the maximum to recovery phase of substorms and rarely in the early expansion phase. It has been further suggested that the occurrence region of suprathermal electron bursts and the substorm activity is closely related. When substorm activity declines and the intensity of *AE*-index decreases below 100 nT, bursts are seen only in the dawn side (see Fig. 12).

As shown in the previous section, we found that the duration time of the bursts is estimated to be less than one orbital period (~100 min) of the DMSP satellite. Using ground-based monochromatic CCD camera data and the DMSP-F6 satellite data, ONO *et al.* (1989) found noticeable precipitation of low-energy electron spikes and showed that such low-energy electrons effectively excite 6300 Å emissions. They observed east-west elongated OI 6300 Å auroral arcs in correspondence with low-energy electron spikes which last for more than few minutes. Since suprathermal electron burst events and low-energy electron spikes have many common features, their result strongly suggests that suprathermal electron bursts also have a spatially east-west elongated sheet-like structure with a narrow latitudinal width rather than regarding them as temporal events.

A close relationship between suprathermal electron bursts and small-scale field-aligned currents found in this paper is important to infer the generation mechanism of suprathermal electron bursts. Using magnetometer and particle data from ISIS-2 spacecraft, MAIER *et al.* (1980) studied FACs associated with suprathermal electrons. They found that both upward and downward suprathermal electron flows can account for the substantial part of the current density inferred from the magnetometer data. HOFFMAN *et al.* (1985) studied on the current carriers for the FAC system using many polar passes of the DE-2 satellite, which covered the whole MLT region in various geomagnetic conditions. Among these passes it was noticed that there are intense (few $\mu Am^{-2}$), small-scale current structures which appear to correspond to suprathermal electron bursts. By comparing particle and magnetometer data, they demonstrated that suprathermal electrons in a few hundred eV energy range can carry about half of the upward current measured by the magnetometer.

In the present paper, we have shown that suprathermal electron bursts carry intense (as much as few $\mu Am^{-2}$), small-scale ($\leq$50 km at $h = 830$ km) upward field-aligned current. Small-scale upward currents are usually embedded in the large-scale region 2 downward current system. As is described before, the fluxes of suprathermal electrons are sufficient to carry these small-scale upward field-aligned currents, while large-scale downward region 2 currents are suggested to be carried by ionospheric thermal electrons flowing away from the ionosphere into the magnetosphere. Then, it is necessary to explain why such intense FACs flow in sharply localized regions in the diffuse aurora region. Our interpretation is as follows. At the time of the substorm expansion, a large amount of electrons and ions flow from the magnetosphere to the ionosphere, intensifying the upward evening region 1 current system. In the evening sector, ionospheric thermal electrons flow into the magnetosphere for carrying downward region 2

currents in the diffuse aurora region. These ionospheric electrons will be heated up to few tens to few hundreds of eV through wave-particle interaction processes in localized regions in the magnetosphere. At the time of the substorm maximum to recovery, those heated electrons precipitate again into the ionosphere, with carrying intense, small-scale upward FACs. Those electrons possibly excite arcs of OI 6300 Å emission. Our interpretation of suprathermal electron bursts is similar to that of MARSHALL *et al.* (1991). They stated that both upward and downward suprathermal bursts observed by DE-1 satellite at high (10,000–20,000 km) altitude in the CPS region result from the diffusive acceleration process acting on cold ionospheric electrons in the magnetosphere. It has now become an interesting problem whether those suprathermal electron bursts in morning sector carry small-scale FACs or not. Since the DMSP-F6 does not carry magnetometer, we can only use the magnetometer data from DMSP-F7 located in the morning sector around 8 h MLT. These data showed that suprathermal electron bursts are embedded in the region 2 upward current region and upward currents are enhanced around the region where suprathermal electron bursts occur. This fact suggests that some different mechanism which drives the FACs of suprathermal electron bursts works in the morning sector.

The authors wish to express sincere thanks to Prof. T. Hirasawa for fruitful discussions and continuous encouragement. The authors are deeply grateful to Mr. K. Uchida of NIPR and the members of the World Data Center-C2 for Aurora for valuable suggestions and help on dealing with the DMSP particle data.

The DMSP-F7 magnetometer data processing was supported by funds from Task 2311G5 of the Air Force Office of Scientific Research.

## APPENDIX

According to the Maxwell's equations, current density vector $\boldsymbol{J}$ is given by

$$\boldsymbol{J} = \frac{1}{\mu_0} \mathrm{rot} \Delta \boldsymbol{B} \tag{A.1}$$

where $\mu_0 = 4\pi \times 10^{-7} = 1.257 \times 10^{-6}$ H m$^{-1}$, the permeability of free space and $\Delta \boldsymbol{B}$ is the magnetic perturbation vector. From Eq. (A.1), we can get the field-aligned current density $J_{\parallel}$ as

$$J_{\parallel} = \frac{1}{\mu_0} \left( \frac{\partial (DBz)}{\partial y} - \frac{\partial (DBy)}{\partial z} \right) \tag{A.2}$$

where $y$ and $z$ represent the Cartesian distance coordinates in the directions $Y$ and $Z$, which are forward and horizontal, cross-track directions of the satellite, respectively.

If we assume that field-aligned currents flow in the form of current sheets with infinite longitudinal extent, the perturbation in $DBy$ component disappears and Eq. (A.2) becomes

$$J_{\parallel} = \frac{1}{\mu_0} \frac{\partial (DBz)}{\partial y}. \tag{A.3}$$

This assumption is close to the actual configuration of field-aligned currents because the perturbations in the $DBz$ component is mostly much larger than those of the $DBy$ component. When we consider the velocity of the DMSP-F7 satellite is ~7.4 km/sec, Eq. (A.3) becomes

$$J_{\parallel} = \frac{1}{\mu_0}\frac{1}{(\partial y/\partial t)}\frac{\partial(DBz)}{\partial t}$$
$$\simeq 0.11 \times \frac{\partial(DBz)}{\partial t} \qquad (A.4)$$

where the units of $J_{\parallel}$, $DBz$, and $t$ are $\mu Am^{-2}$, nT, and sec, respectively. From Eq. (A.3), the magnitude of the current intensity $\int J_{\parallel} dy$ is given directly by the amplitude of the magnetic disturbance $DBz$ by

$$\int J_{\parallel} dy = \frac{1}{\mu_0} DBz$$
$$\simeq 8.0 \times 10^{-4} \times DBz \qquad (A.5)$$

where the unit of $\int J_{\parallel} dy$ is A $m^{-1}$.

By applying the $DBz$ component of SSM data to Eq. (A.4), we can estimate the field-aligned current density $J_{\parallel}$.

## REFERENCES


ARNOLDY, R. L., T. E. MOORE, and L. J. CAHILL, Jr., Low-altitude field-aligned electrons, *J. Geophys. Res.*, **90**, 8445–8460, 1985.

COLLIN, H. L., R. D. SHARP, and E. G. SHELLEY, The occurrence and characteristics of electron beams over the polar regions, *J. Geophys. Res.*, **87**, 7504–7511, 1982.

DOERING, J. P., T. A. POTEMRA, W. K. PETERSON, and C. O. BOSTROM, Characteristic energy spectra of 1- to 500-eV electrons observed in the high-latitude ionosphere from Atmosphere Explorer C, *J. Geophys. Res.*, **81**, 5507–5516, 1976.

EATHER, R. H., DMSP calibration, *J. Geophys. Res.*, **84**, 4134–4144, 1979.

FELDSTEIN, Y. I., Peculiarities in the auroral distribution and magnetic disturbance distribution in high latitudes caused by the asymmetrical form of the magnetosphere, *Planet. Space Sci.*, **14**, 121–130, 1966.

GUSSENHOVEN, M. S., D. A. HARDY, and N. HEINEMANN, Systematics of the equatorward diffuse auroral boundary, *J. Geophys. Res.*, **88**, 5692–5708, 1983.

HARDY, D. A., L. K. SCHMITT, M. S. GUSSENHOVEN, F. J. MARSHALL, H. C. YEH, T. L. SCHUMAKER, A. HUBER, and J. PANTAZIS, Precipitating electron and ion detectors (SSJ/4) for the block 5D/flights 6–10 DMSP satellites: calibration and data presentation, Rep. *AFGL-TR-84-0317, Air Force Geophys. Lab., Hanscom Air Force Base*, Mass., 1984.

HARDY, D. A., M. S. GUSSENHOVEN, and E. HOLEMAN, A statistical model of auroral electron precipitation, *J. Geophys. Res.*, **90**, 4229–4248, 1985.

HOFFMAN, R. A., M. SUGIURA, and N. C. MAYNARD, Current carriers for the field-aligned current system, *Adv. Space Res.*, **5**, 109–126, 1985.

IIJIMA, T. and T. A. POTEMRA, The amplitude distribution of field-aligned currents at northern high latitudes observed by Triad, *J. Geophys. Res.*, **81**, 2165–2174, 1976.

JOHNSTONE, A. D. and J. D. WINNINGHAM, Satellite observations of suprathermal electron bursts, *J. Geophys. Res.*, **87**, 2321–2329, 1982.

LIN, C. S., J. L. BURCH, J. D. WINNINGHAM, J. D. MENIETTI, and R. A. HOFFMAN, DE-1 observations of counterstreaming electrons at high altitudes, *Geophys. Res. Lett.*, **9**, 925–928, 1982.

LU, G., P. H. REIFF, J. L. BURCH, and J. D. WINNINGHAM, On the auroral current-voltage relationship, *J. Geophys. Res.*, **96**, 3523–3531, 1991.

MAIER, E. J., S. E. KAYSER, J. R. BURROWS, and D. M. KLUMPAR, The suprathermal electron contributions to high-latitude Birkeland currents, *J. Geophys. Res.*, **85**, 2003–2010, 1980.

MARSHALL, J. A., J. L. BURCH, J. R. KAN, P. H. REIFF, and J. A. SLAVIN, Sources of field-aligned currents in the auroral plasma, *Geophys. Res. Lett.*, **18**, 45–48, 1991.

ONO, T., T. HIRASAWA, and C.-I. MENG, Weak auroral emissions and particle precipitations in the dusk auroral oval, *J. Geophys. Res.*, **94**, 11933–11947, 1989.

RAITT, W. J. and J. J. SOJKA, Field-aligned suprathermal electron fluxes below 270 km in the auroral zone, *Planet. Space Sci.*, **25**, 5–13, 1977.

RICH, F. J., Fluxgate magnetometer (SSM) for the defense meteorological satellite program (DMSP) block 5D-2, flight 7, Rep. AFGL-TR-84-0225, Air Force Geophys. Lab., Hanscom Air Force Base, Mass., 1984.

ROBINSON, R. M., J. D. WINNINGHAM, J. R. SHARBER, J. L. BURCH, and R. HEELIS, Plasma and field properties of suprathermal electron bursts, *J. Geophys. Res.*, **94**, 12031–12036, 1989.

SANDAHL, I. and P.-A. LINDQVIST, Electron populations above the nightside auroral oval during magnetic quiet times, *Planet. Space Sci.*, **38**, 1031–1049, 1990.

SHARP, R. D., E. G. SHELLEY, R. G. JOHNSON, and A. G. GHIELMETTI, Counterstreaming electron beams at altitudes of ~1 $R_E$ over the auroral zone, *J. Geophys. Res.*, **85**, 92–100, 1980.

TANSKANEN, P. J., D. A. HARDY, and W. J. BURKE, Spectral characteristics of precipitating electrons associated with visible aurora in the premidnight oval during periods of substorm activity, *J. Geophys. Res.*, **86**, 1379–1395, 1981.

WINNINGHAM, J. D., F. YASUHARA, S.-I. AKASOFU, and W. J. HEIKKILA, The latitudinal morphology of 10-eV to 10-keV electron fluxes during magnetically quiet and disturbed times in the 2100–0300 MLT sector, *J. Geophys. Res.*, **80**, 3148–3171, 1975.